Smart Mater. Struct. **19** (2010) 035028 (11pp) doi:10.1088/0964-1726/19/3/035028

Experimental implementation of acoustic impedance control by a 2D network of distributed smart cells

P David, M Collet and J-M Cote

DMA, FEMTO-ST, 24 rue de l'Épitaphe, 25000 Besançon, France

E-mail: manuel.collet@univ-fcomte.fr

Received 16 December 2009
Published 11 February 2010
Online at stacks.iop.org/SMS/19/035028

Abstract

New miniaturization and integration capabilities available from emerging microelectromechanical system (MEMS) technology will allow silicon-based artificial skins involving thousands of elementary actuators to be developed in the near future. Smart structures combining large arrays of elementary motion pixels are thus being studied so that fundamental properties could be dynamically adjusted.

This paper investigates the acoustical capabilities of a network of distributed transducers connected with a suitable controlling strategy. The research aims at designing an integrated active interface for sound attenuation by using suitable changes of acoustical impedance. The control strategy is based on partial differential equations (PDE) and the multiscaled physics of electromechanical elements. Specific techniques based on PDE control theory have provided a simple boundary control equation able to annihilate the reflections of acoustic waves.

To experimentally implement the method, the control strategy is discretized as a first order time–space operator. The obtained quasi-collocated architecture, composed of a large number of sensors and actuators, provides high robustness and stability. The experimental results demonstrate how a well controlled active skin can substantially modify sound reflectivity of the acoustical interface and reduce the propagation of acoustic waves.

(Some figures in this article are in colour only in the electronic version)

1. Introduction

In contrast to passive systems [1–3], an ANC (active noise control) system may be much smaller and lighter, even for low frequency applications, but it loses its efficiency and stability at higher frequencies. A suitable combination of active and passive methods allows us to achieve an interesting compromise between dimensions, weight, and efficiency, and the resulting system proposes better performance over a wide frequency range [4].

Common ANC strategies, comprising *local* and *global* approaches, generally using some kind of adaptive feedback or feedforward algorithm, have been enriched in recent years by active acoustical impedance control [5, 6]. While local control methods consist basically in pressure suppression at particular locations predefined by the placement of error microphones, global methods deal with the reduction of the overall acoustic energy or radiated power of the primary source [7]. Both previous strategies act directly on the acoustical medium by using secondary sources, while the impedance control methodology tends to adjust the acoustical properties of boundary interfaces to induce suitable sound diffusion. However, the implementation of impedance control appears to be very complex due to the necessity of knowing not only the pressure, but also the corresponding velocity at the controlled point.

The classical approaches [5, 8] used by many authors studying the implementation of active acoustic impedance, such as Galland *et al* [9, 10] for example, are based on the knowledge of the so-called optimal complex impedance, which they tend to implement experimentally using hybrid parietal ANC systems. Their purpose is to locally control a boundary interface to follow the pre-established frequency-dependent complex impedance. Indeed, the total absorption of normal incident waves is described by the simple impedance value $Z = \rho_0 c_0$, where ρ_0 is the density of air and c_0 is the speed

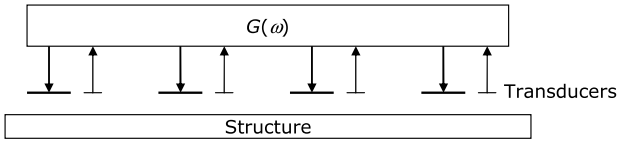

Figure 1. Centralized control system.

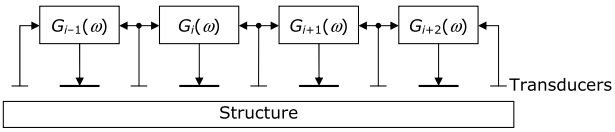

Figure 2. Distributed quasi-collocated system of the 1st order.

of sound in air. However, since the acoustic waves are not always normally incident, this simple absorption condition has to be modified. The proposed solutions for impedance optimization [9, 10] lead to theoretical frequency-dependent impedances $Z(\mathrm{j}\omega)$ guaranteeing efficient sound absorption and depending on disturbances, boundary conditions, speed of sound, frequency band, structural interfaces, and geometry. These dependencies prohibit applications in the broadband frequency range and good efficiency is restricted to a specific configuration.

The optimally designed impedance [9, 10] is a frequency-dependent function $Z(\mathrm{j}\omega)$, linking acoustic pressure and velocity. While its experimental implementation allows the control of these parietal quantities by using only the corresponding time operator, it also appears very interesting to introduce a wavenumber dependency so that $Z = Z(\mathrm{j}\omega, \mathrm{j}k)$, in order to improve efficiency and versatility [11, 12]. The real-time implementation of such an optimal boundary control involves a complex partial differential operator, with not only time but also space derivatives [13]. This approach requires a large amount of system resources (memory and processing speed) and therefore the use of a classical centralized controller (figure 1) is not suitable for practical applications.

To overcome the disadvantages of a centralized system, let us consider the system given in figure 2. It represents a fluid–structure interface covered by a network of sensors and actuators that are connected by an *ad hoc* electronic circuit. The scheme describes a first order system where signals from two neighbouring sensors are used to control one actuator. This co-localized configuration allows implementation of a complete generalized acoustical impedance $Z(\mathrm{j}\omega, \mathrm{j}k)$ involving a first order space operator.

The optimization problem here is to confer acoustic absorption properties on this active surface so that all incident waves, intercepted by the interface under any angle, are reflected the least possible. If the wave is normally incident a simple wall impedance $\rho_0 c_0$ is obtained. In other cases the impedance is much more complex and known only in the mathematical form of a pseudo-differential operator [12]. The quasi-co-localization between sensors and actuators (figure 2) avoids a robustness problem inherent in closed-loop systems so that the performance and efficiency can be focused. The effectiveness of the system depends mainly on the transducers

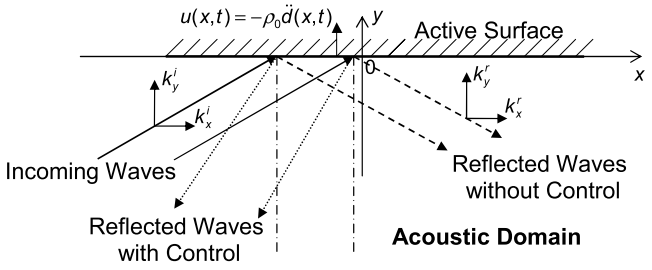

Figure 3. Acoustic waves interacting with the active surface.

used but also on the control law connecting them. This law must be distributed in order to avoid the signal dephasing induced by the time delay when a large number of acquisition/control channels is used in the centralized system.

This paper is divided in three parts. The introduction presents a brief summary of active noise control (ANC) methods in the context of acoustical impedance modifications. Section 2 introduces generic methodology for computing a generalized acoustical impedance operator for total absorption of acoustic waves along a straight interface. The obtained complex operator contains space and time differential terms that are discretized in order to implement the control strategy experimentally. The great potential of the method is demonstrated on a simple example with a plane-wave tube, and the numerical modelling is compared with the experimentally obtained results. Finally, section 3 presents the development of a network with a large number of individual smart cells interconnected with the proposed control law. Some experimental results are presented to demonstrate the attenuation capabilities of such an integrated system.

2. Active impedance boundary control

Derivation of the control law is presented in this article only in a short form, more detailed investigation can be found in [14]. Instead of presenting the formal definition of a absorbing boundary operator (generalized impedance operator), we consider the total absorption of acoustic energy contained in a half-plane by optimizing the boundary impedance. This allows us to present a new methodology for designing an interface control strategy on a simple example, nevertheless, the proposed method can be extrapolated to complex systems.

2.1. Control problem

First of all let us consider the problem in two dimensions described by the following equations representing the vibroacoustic system in figure 3, where $u(x,t)$ is the control parameter and $m(x,t)$ is the measured variable:

$$\frac{1}{{c_0}^2}\frac{\partial^2 p}{\partial t^2} - \Delta p = 0 \qquad \text{on } \mathbb{R}_x \times \mathbb{R}_y^{-*} \times \mathbb{R}_t^{*+}, \tag{1a}$$

$$\frac{\partial p(x,0,t)}{\partial y} = u(x,t), \tag{1b}$$

$$m(x,t) = p(x,0,t). \tag{1c}$$

The system is described by the wave equation (1*a*) and the measured parameter $m(x,t)$ is the parietal acoustic pressure (i.e. $p(x,0,t)$). The control variable $u(x,t)$ is a normal derivative of the acoustic pressure on the control boundary (i.e. $\frac{\partial p(x,0,t)}{\partial y}$). This can be interpreted as a velocity of the active surface interacting with the air. As indicated in figure 3, $u(x,t)$ is proportional to the normal acceleration $\ddot{d}(x,t)$ of the active surface.

We could seek to define a relation $u(x,0,t) = G[m(x,t)]$ such that the acoustic waves on the boundary $y = 0$ are totally absorbed by the active interface. This type of control is asymptotically stable because the energy inside the acoustic domain can only decrease. In general case, the control function for total absorption is given by the following equation [14]:

$$u = G(k_x,\omega)m = -2\pi\sqrt{{k_x}^2 - \frac{\omega^2}{{c_0}^2}}m. \tag{2}$$

The pseudo-differential operator corresponding to the control equation (2) is $-\sqrt{\partial_y^2 - \partial_t^2}$. The interface impedance relationship implies a total wave absorption. This operator is pseudo-differential, non-local in time and space, and also appears difficult to implement on a realistic system. Different mathematical techniques have been introduced for the numerical realization of such pseudo-differential operators as the diffusive representations, presented in the work of Matignon *et al* [11]. A concrete realization of such a generalized impedance in real-time through a suitable distributed active system is today unrealistic because of the number and the complexity of necessary calculations. A large part of the research in this domain deals with the implementation of diffusive representations and simplifications that could be carried out [15].

2.2. Control strategy

The objective of the strategy used is to induce a reflection of the waves intercepted by the active surface so that the reflected wavenumbers k_x^r are negative. The incidental acoustic energy is thus sent back towards the negative x and the acoustic power flow in the domain is reduced. This condition can be directly extended to control acoustic waves in a tube. The adopted control operator defined in equation (2) is represented by the following transport formulation (advection equation) directed to the negative x:

$$u(x,t) = -\left(\frac{1}{c_a}\frac{\partial m(x,t)}{\partial t} - \frac{\partial m(x,t)}{\partial x}\right), \tag{3}$$

where c_a represents the transportation velocity, which stands for the control parameter and its optimal value is $c_a = c_0$ [14]. We seek to impose a solid-state transport with only one direction of propagation. This direction is obviously contrary to that for which we want to minimize the transmittance. This coupling induces only evanescent waves propagating toward the positive x direction, thereby avoiding the existence of any concordance frequency.

By combining equations (1) and (3) and by symmetrization of the system, the controlled behaviour is described by the following equations:

$$\frac{1}{{c_0}^2}\frac{\partial^2 p}{\partial t^2} - \Delta p = 2\delta(y)\left(\frac{1}{c_a}\frac{\partial m(x,t)}{\partial t} - \frac{\partial m(x,t)}{\partial x}\right) \quad \text{on } \mathbb{R}_x \times \mathbb{R}_y \times \mathbb{R}_t^{*+}, \tag{4a}$$

$$m(x,t) = p(x,0,t), \tag{4b}$$

$$+ \text{ initial conditions.} \tag{4c}$$

Using the Fourier transforms in time and space, the solution of the system (4) implies that the Fourier transform of the parietal pressure along the active boundary

$$\tilde{m}(k_x,\omega) = \tilde{m}(k_x,\omega)\frac{\mathrm{j}\left(\frac{\omega}{c_a} - k_x\right)}{\sqrt{{k_x}^2 - \frac{\omega^2}{{c_0}^2}}}. \tag{5}$$

So, a non-zero solution exists if and only if

$$\mathrm{j}\left(\frac{\omega}{c_a} - k_x\right) = \sqrt{{k_x}^2 - \frac{\omega^2}{{c_0}^2}} \tag{6}$$

so we get the sufficient condition

$$2{k_x}^2 - \frac{2k_x\omega}{c_a} + \left(\frac{1}{{c_a}^2} - \frac{1}{{c_0}^2}\right)\omega^2 = 0. \tag{7}$$

Thus, if we choose the control parameter c_a such that ${c_a}^2 \geqslant {c_0}^2/2$, we obtain waves with $k_x > 0$ whatever the frequency ω and the incidence angle [14]. The obtained active skin behavior also yields a very promising generalized impedance that could be used for acoustic power flow control. The design interface behavior is created by using a standard first order differential operator in time and space (3) that can be discretized and implemented through a distributed set of unit cells. In the next section, the proposed control strategy is implemented on a simple plane-wave tube.

2.3. Implementation in a tube

The acoustic system shown in figure 4 represents a simple implementation of the control law in a plane-wave tube. The active zone is composed alternately of seven circumferences of actuators and eight circumferences of sensors. These transducer channels are, in fact, implemented by a parallel distribution of four loudspeakers and four microphones.

Each row of circumferential loudspeakers is controlled by a uniquely applied signal computed by using two measurements picked up by the two adjacent rows of microphones (see figure 2). This distribution allows us to implement a discrete version of the control law given by equation (3). The problem is firstly investigated numerically and the results are then compared with experiments. Only a brief view on the problem is given in this paper with some numerical and experimental results. A more detailed study of the system can be found in [14].

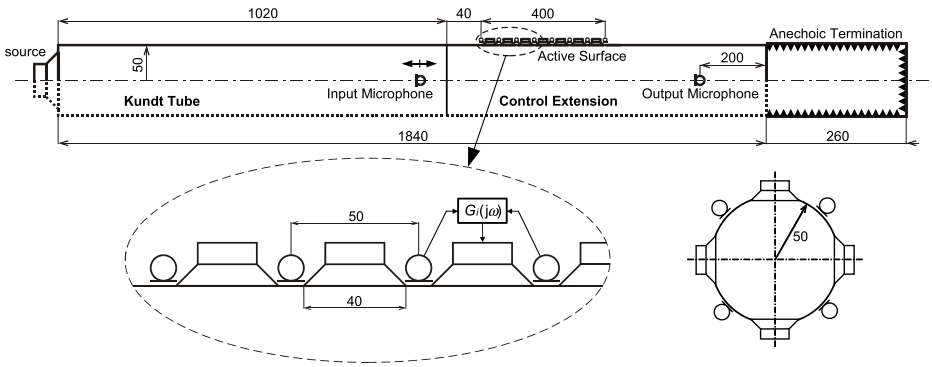

Figure 4. Modelled vibroacoustic system.

2.3.1. Modelling of fluid–structure interaction. Modelling of fluid–structure interaction is introduced as an influence of the controlled boundary on the surrounding air. The electromechanical coupling effects and the internal dynamics of corresponding internal modes of the loudspeaker's membranes are modelled by the following equation [14]:

$$\bar{\rho}_{\mathrm{sp}}\ddot{d}_i + c_{\mathrm{sp}}\dot{d}_i + k_{\mathrm{sp}}d_i + T_{\mathrm{sp}}\Delta d_i = p\cdot l_{\mathrm{sp}} + g_e v_i, \qquad (8)$$

where $\bar{\rho}_{\mathrm{sp}}$ is the linear mass distribution of the membrane under a tension of T_{sp}, k_{sp} is the linear distribution of stiffness and c_{sp} is the damping coefficient of the membrane. These mechanical characteristics have been determined from measurements of the micro-loudspeakers used. The external forces are induced by the pressure p exerted over the actuator's length l_{sp} and by the electrodynamic control efforts $g_e v_i$ (g_e represents the static gain of the corresponding electromechanical coupling and v_i is the injected voltage).

The global system of PDEs driving the whole coupled axisymmetric problem (fluid, structure, and loudspeaker) is given by the following equations:

$$\frac{y}{c_0^2}\frac{\partial^2 p}{\partial t^2} - \left[\frac{\partial}{\partial y}\left(y\frac{\partial p}{\partial y}\right) + \frac{\partial}{\partial x}\left(y\frac{\partial p}{\partial x}\right)\right] = 0 \quad \text{on } \Omega \times \mathbb{R}_t^{*+}, \qquad (9a)$$

$$\frac{\partial p(0,y,t)}{\partial x} = \frac{\omega}{c_0}p_c \qquad \text{on } \Gamma_{\mathrm{in}} \times \mathbb{R}_t^{*+}, \qquad (9b)$$

$$\frac{\partial p(x,R,t)}{\partial y} = -\rho_0 \ddot{d}_i(x,t) \qquad \text{on } \Gamma_i \times \mathbb{R}_t^{*+}, \qquad (9c)$$

$$\frac{\partial p(x,R,t)}{\partial y} = 0 \qquad \text{on } \Gamma_R \times \mathbb{R}_t^{*+}, \qquad (9d)$$

$$\frac{\partial p(L,y,t)}{\partial x} = -\frac{1}{c_0}\frac{\partial p}{\partial t} \qquad \text{on } \Gamma_{\mathrm{out}} \times \mathbb{R}_t^{*+}, \qquad (9e)$$

$$\frac{\partial p(x,0,t)}{\partial y} = 0 \qquad \text{on } \Gamma_{\mathrm{sym}} \times \mathbb{R}_t^{*+}, \qquad (9f)$$

$$\bar{\rho}_{\mathrm{sp}}\ddot{d}_i + c_{\mathrm{sp}}\dot{d}_i + k_{\mathrm{sp}}d_i + T_{\mathrm{sp}}\Delta d_i = p l_{\mathrm{sp}} + g_e v_i \quad \text{on } \Gamma_i \times \mathbb{R}_t^{*+}. \qquad (9g)$$

$p_c = 20$ Pa is the acoustic pressure on the input boundary Γ_{in} on the left side, R is the radius and L is the length of the tube, Γ_i is the membrane boundary corresponding to the ith loudspeaker, Γ_R is a rigid wall, Γ_{out} is the Sommerfeld radiation boundary on the right side of the tube, and Γ_{sym} is the symmetry boundary.

2.3.2. Discrete form of the control equation. The continuous control equation (3) theoretically developed for a 2D semi-infinite domain can be directly applied to control the acoustical flow in the tube. However, to implement the equations onto the distributed set of acoustic transducers, the control law has to be discretized. The spatial discretization of the measured pressure in equation (3) is introduced so that $p(i\mathrm{d}x,t) = p_i$ and the time discretization is given by $\partial p(i\mathrm{d}x,t)/\partial t = \dot{p}_i$. The spatial discretization depends on the distance between each row of microphones, in our case $dx = 0.05$ m and the actuator length is $l_{\mathrm{sp}} = 0.04$ m. A simple first order Euler approximation scheme of the involved space operator is applied to obtain the control law in the discrete form:

$$\frac{\partial p(x,R,t)}{\partial y} = -\left(\frac{1}{c_a}\frac{\dot{p}_{i+1}+\dot{p}_i}{2} - \frac{p_{i+1}-p_i}{dx}\right) \quad \text{for } x \in [i\,dx, (i+1)dx]. \qquad (10)$$

The discretization step $dx = 5$ cm introduces a numerical limitation at a frequency around 3400 Hz, but the time delay of the control loop is even more important parameter which considerably reduces the frequency ceiling.

By assuming a monomodal response of loudspeakers, one can directly compute the imposed control voltage $v_{\mathrm{i}}(t)$ so that relation (10) is satisfied, hence;

$$v_i(t) = -\frac{l_{\mathrm{sp}}}{g_e}\left(\frac{p_{i+1}+p_i}{2}\right) + \frac{M_{\mathrm{sp}}}{\rho_0 g_e l_{\mathrm{sp}}}\left[\frac{1}{c_a}D\left(\frac{p_{i+1}+p_i}{2}\right) - \frac{p_{i+1}-p_i}{dx}\right], \qquad (11)$$

D denotes a simple derivative filter to introduce the time derivative operator by the following transfer function:

$$H_D(s) = \frac{{\omega_D}^3 s}{(s+\omega_D)^3}, \qquad (12)$$

where ω_D is a suitably chosen optimization parameter.

2.3.3. Numerical results. The system of equations (9) has been modelled with COMSOL Multiphysics™ software and the postprocessing has been treated in MATLAB® to obtain the frequency response of the controlled system. The used finite element mesh is discretized so that the element size does not exceed $\lambda_{\mathrm{lim}}/4$, where $\lambda_{\mathrm{lim}} = c_0/f_{\mathrm{lim}}$, $f_{\mathrm{lim}} = 3$ kHz. It is important to note that the obtained system is numerically

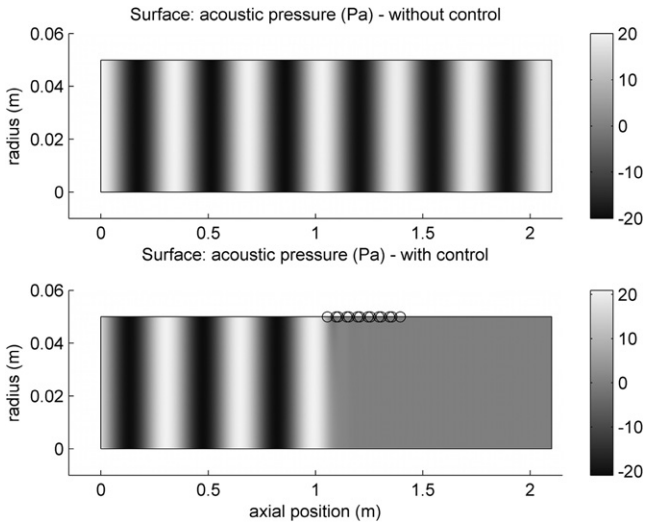

Figure 5. Controlled and uncontrolled pressure distribution, frequency 1000 Hz.

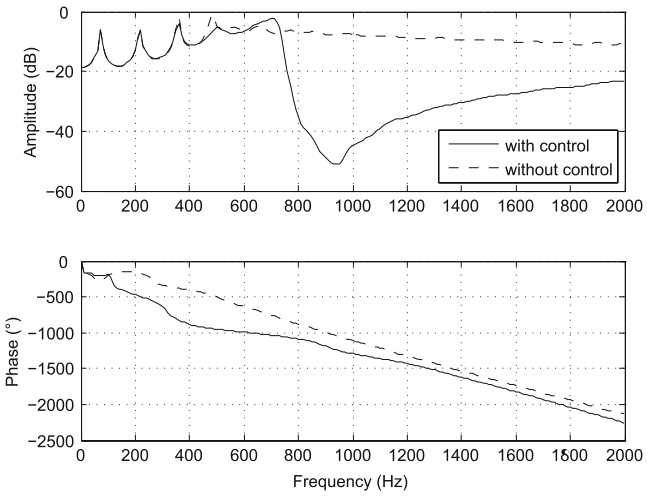

Figure 6. Transfer function between the input and output acoustic pressure, numerical results.

stable. The harmonic calculations have been carried out in the frequency range 0–2000 Hz with a 10 Hz step. Figure 5 shows the pressure field corresponding to the frequency of 1000 Hz, where the control is the most efficient.

The Bode diagram in figure 6 represents the acoustic transfer function between the pressure gradient at the source loudspeaker and the acoustic pressure at the output microphone. We note that the system effectiveness is very good in the range of 700–2000 Hz, with significant loss of attenuation even above the frequency limit of plane waves in the tube $f_p \approx 1700$ Hz. The attenuation of sound levels rises up to 40 dB at 950 Hz. The considerable damping rate of transducers at the first suspension mode (800 Hz) allows the loudspeaker's membranes to passively absorb energy contained in the frequency band around that of resonance.

It is necessary to underline here that the internal stiffness of the control loudspeakers is a very important dimensioning parameter that makes it possible to qualify the frequency band of the system. It affects the control effectiveness, in particular, compared to *spillover* problems and must be as large as possible.

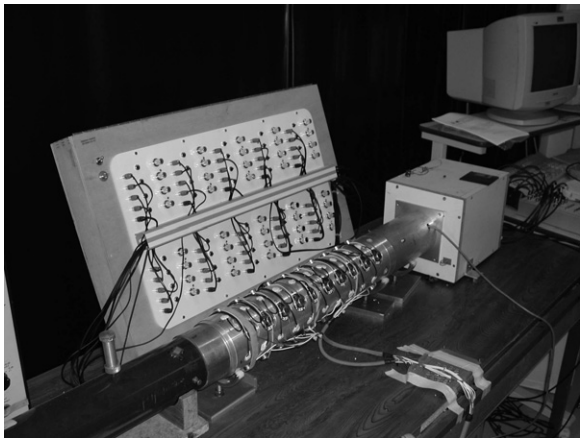

Figure 7. Experimental set-up.

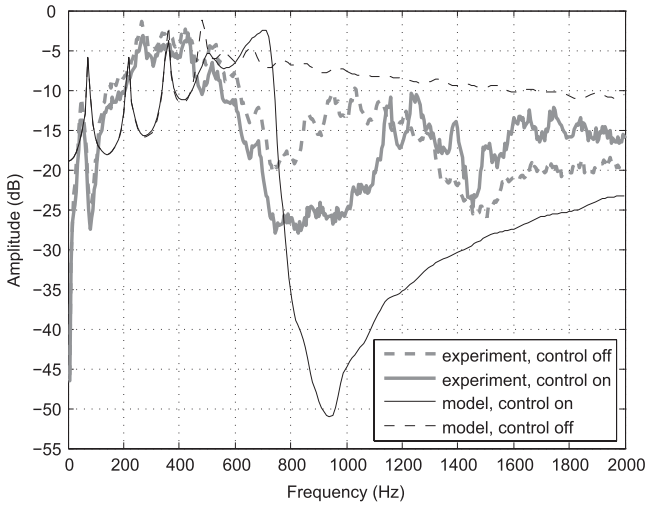

Figure 8. Comparison of transfer functions obtained numerically and experimentally.

2.3.4. Experimental results. The breadboard construction carried out in our laboratory, shown in figure 7, implements exactly the control equations that have been tested numerically. In practice, the real properties of the employed loudspeakers reduced the frequency band with great effectiveness between 700 and 1200 Hz. The limitations are due to the mechanical characteristics of the transducers, especially their first internal eigenmode at 800 Hz. The upper frequency limit at 1200 Hz is caused by the phase lag introduced by time delay of the used signal processor. Our hardware resources (dSPACE® DS1104 R&D Controller Board) provided seven channels of control loudspeakers and eight channels of microphones to implement the control strategy. Figure 8 compares the numerical results with the measured transfer function between the signal of disturbance applied to the input loudspeaker and the acoustic pressure measured at the output of the tube.

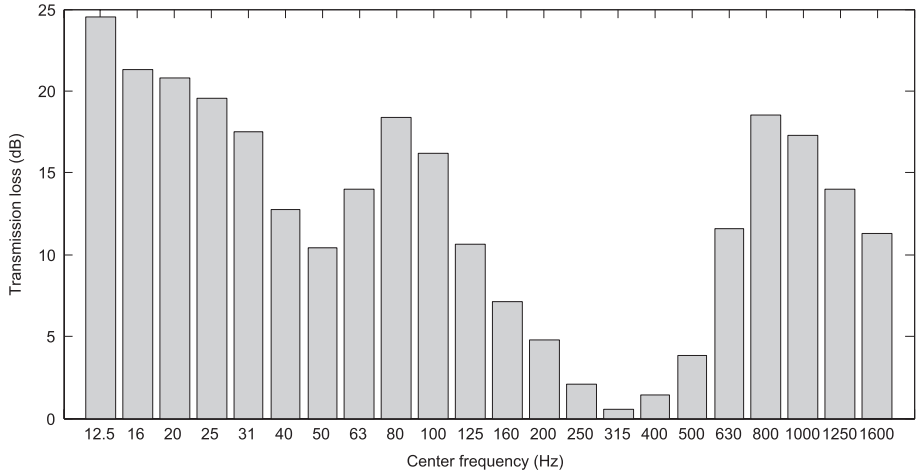

Figure 9. Sound transmission loss in 1/3 octave bands, experimental results.

Although there is not a perfect correlation between the experimental and numerical results, one qualitatively observes the correct operation of the system compared to the numerical results. The reduction in the acoustic transfer is broadband and the form of the system response is comparable to that obtained theoretically. The amplitude peaks on the experimental curves are caused by a non-ideal anechoic termination, and their frequencies correspond to the stationary wave modes in the tube.

The main aim of this study was not to realize a precise model of the plane-wave tube with our 'handmade' anechoic termination but to qualify the control strategy. It is possible to update the passive behaviour of the numerical model by using experimental data but this work has not been carried out at this stage. Moreover, the simplified model we used allowed us to illustrate the main physical characteristic of the controlled system and to identify the most important design variables: suspension eigenfrequency, time delay of the control loop, transducer's discretization, internal dynamics of the control speakers, etc, which are the basic constraints limiting the efficient frequency band of this adaptive acoustical skin.

The transmission loss is defined as the difference in decibels between the levels of incoming acoustic power upstream and outgoing power downstream when the acoustic treatment is turned on. If reflections of acoustic waves are neglected and only plane waves are assumed, the sound transmission loss can be written as [16]

$$\mathrm{TL} = 20 \log \frac{p_{\mathrm{in}}}{p_{\mathrm{out}}}, \tag{13}$$

where p_{in} and p_{out} are the acoustic pressures upstream and downstream respectively. The sound transmission loss given by equation (13) is presented in figure 9 in third-octave bands. The plane waves frequency limit for the this experimental device is 1715 Hz. Relatively high attenuations at low frequencies are caused by the standing waves, which appear even when the control system is turned off.

The applied experimental tests confirm the expected functionality in the efficient frequency band without any instability problems. The use of low quality transducers and other electronic components underlines the high robustness of this distributed strategy, which appears as a fundamental property.

Moreover, it has been revealed that the efficient frequency band, here from 700 to 1200 Hz, depends mainly on the time delay of the control loop and on the experimental space discretization of the transducers. Section 3 is dedicated to refine the test bench in order to show up experimentally the influence of the space distribution on the effectiveness of the system.

3. Active antinoise skin

Completely decentralized implementation of the control strategy with microcomponent technologies is studied in this section. In fact, for the control of audible frequencies, there is no necessity of very high discretization of the transducers network involving microelectromechanical system technology. We need, however, the capability of designing highly integrated electroacoustical devices comprising not only transducers (microphones and loudspeakers) but also a distributed numerical control, enabling an improvement in the architecture and properties, compared to the centralized system. The microelectronic or MEMS technology in this study is not important for developing the transducers but for integrating the control electronics in each separate cell.

The proposed decentralized system is represented by 2D network of individual active cells. Each of these cells integrates its own microcontroller, sensor and actuator, amplifiers and signal conditioning. Implementation of the used control strategy requires that each cell uses its own sensor and the signals from sensors of neighbouring cells. A schematic representation of the network is presented in figure 10. Each actuator is located in the centre between four surrounding sensors. By simple modification of the program introduced to the microcontroller of each cell, it is possible to define the direction of acoustic waves to be controlled (horizontal, vertical and even diagonal orientation). The design includes one *master* microcontroller to program the whole set of active

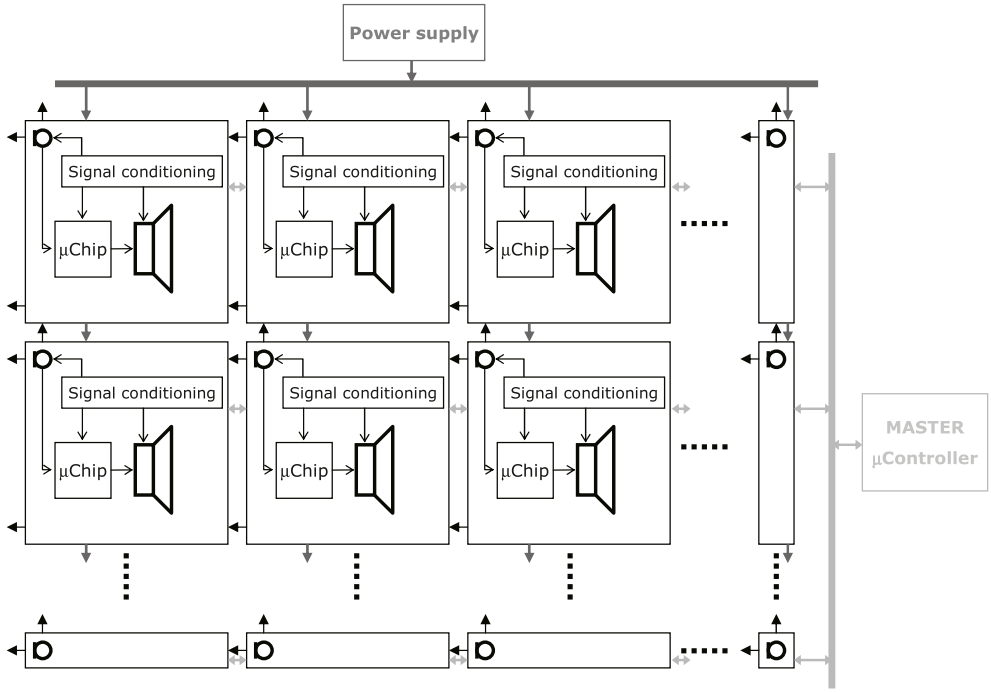

Figure 10. Schematic view of the network design.

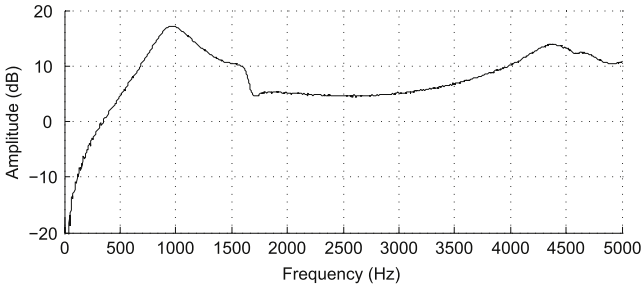

Figure 11. Frequency response of the control speaker's membrane.

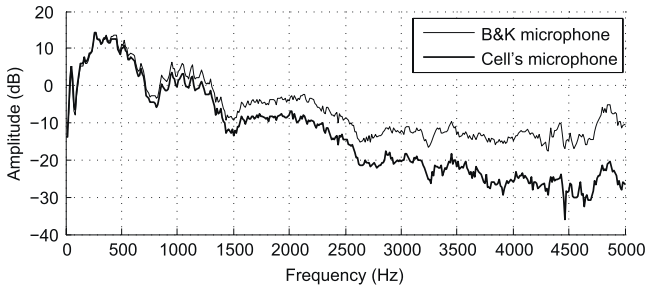

Figure 12. Comparison of the used miniature microphone with a precision reference microphone.

cells and access the input and output signals of any cell, however, this part has not been yet implemented because of its great complexity and processing speed requirements.

3.1. Choice of electronic components

The principal condition for choosing the used components was their dimensions, because of the relatively small space discretization of 30 mm with a theoretical frequency limit of 6.5 kHz. After measuring the frequency responses of several electrodynamic and piezoelectric speakers, a micro-loudspeaker 0.3 W/8 Ω used generally in telecommunication devices was chosen for its best performance/size ratio, however its resonant frequency at 750 Hz cannot offer a significant attenuation at low frequencies. Figure 11 shows the frequency response of the speaker's membrane measured by a laser vibrometer. The speaker has been demounted to access its membrane with a vibrometer when excited by white noise. The choice of the employed miniature microphone 2.2 kΩ/2 V was based simply on its size and linearity requirements in the considered frequency band. The transfer function measured in the plane-wave tube using the used miniature microphone is compared in figure 12 to that obtained by a precision capacitive reference microphone. The differences in frequency response are due to the loss of sensitivity of the miniature microphone at higher frequencies, but the change is linear across the frequency band.

Several parameters of different microcontrollers have been identified before choosing the computing unit for each of active cells. An analysis of principal constraints such as speed, dimensions and resolution of numerical conversion has led to the final choice of an ADuC7026. This 16-bit microchip offers 40×10^6 instructions per second, 12-bit A/D and D/A converters, fast programming in C and very small dimensions. Figure 13 shows the measured A/D and D/A conversion linearity of the microcontroller. The output signal is limited by the programming procedure used to avoid amplitude saturation.

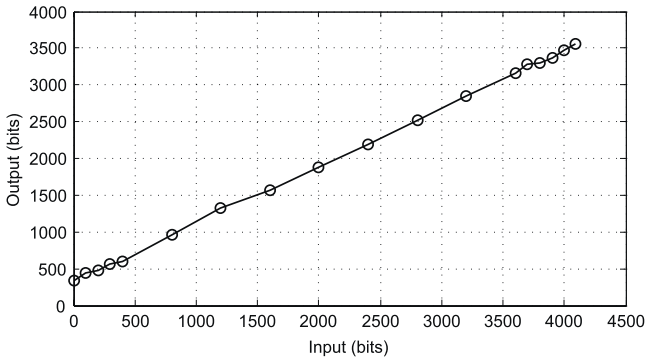

Figure 13. Linearity of the microcontroller's converters.

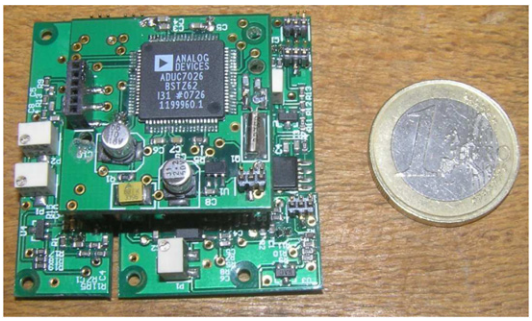

Figure 15. Underside of the cell.

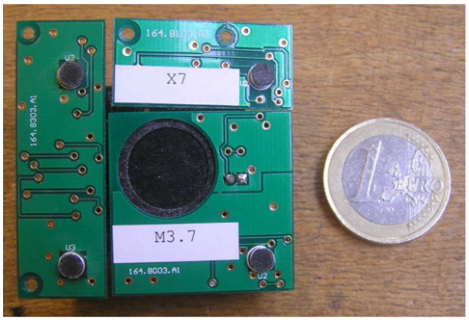

Figure 14. Face side of the cell.

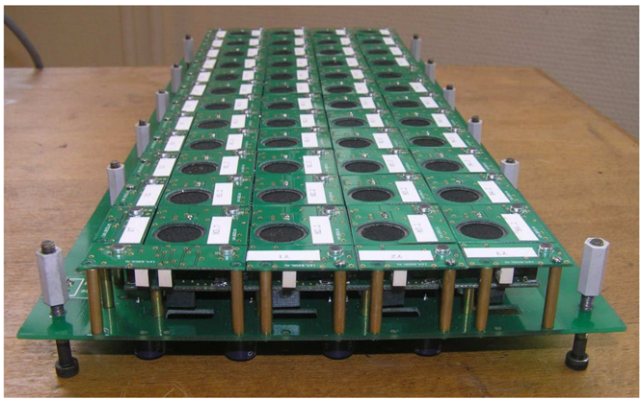

Figure 16. General view of 4 × 12 cells.

3.2. Network development

The small space discretization given by 30 mm distance between sensors offers a theoretical frequency limit at 6.5 kHz. This small spacing results in a high degree of miniaturization to allow the fabrication of a network with a large number of cells. Two identical control devices have been built, each composed of 4 × 12 cells, giving (9 × 36) cm of active surface. Each cell can be deactivated separately and all input and output signals and the microphone's calibrating potentiometers can be accessed. Both devices are composed of three layers: (1) a supporting layer with power supply, mechanical support and fixation system; (2) a computing layer with the microcontroller and (3) an active layer with transducers and their supporting circuits (amplifiers and signal conditioning). In figures 14–16 are close-ups of one cell and a general view of the assembled active device.

The experimental set-up is composed of a chipboard tube with rectangular cross-section, an audio amplifier with source loudspeaker on the input, two devices with active surfaces and non-reflecting acoustic termination on the output. The general view of the measurement device is presented in figure 17. The wooden material offers sufficient rigidity and robustness while offering simplicity to work with. The inner dimensions of the tube are (90 × 135 × 1500) mm. It consists of three separable segments that facilitate the demounting or replacement of the active surface. The primary excitation is made by a quality loudspeaker with 8 cm diameter. The acoustically transparent termination at the output of the tube reduces the effect of eigenmodes caused by internal steady waves. As the first transversal mode eigenfrequency is at 1270 Hz, the measurement device is theoretically prepared for controlling even non-plane waves.

3.3. Validation of the cells

Firstly, all cells have been demounted and each microphone has been calibrated with a pistonphone to the level of 76 dB. Then, the control law has been sent into one of the cells and the output on the control speaker has been tested. Sinusoidal signals of the same frequency but with different phase shift on the microphones have permitted the validation of the output signal. After several program adjustments, the correct form and phase of the output signal have been found. The time delay of the control loop, caused mainly by four successive A/D conversions of the input signals from the microphones, has been identified as 90 μs. This period corresponds approximately to 11 kHz and consequently, the output signal from the controller is entirely in opposition of phase for frequencies around 5.5 kHz. However, the signal de-phasing is already large enough at 2.5 kHz and the efficiency loss of the control algorithm is expected even below this limit.

In the next step, the network has been assembled and inserted in the tube. With a sinusoidal excitation of several frequencies on the input loudspeaker, all microphone signals have been displayed on the oscilloscope. Each cell has then been programmed to identify the global behaviour of the system. Figure 18 presents a progressive amplitude reduction and phase change as the primary 1 kHz sinusoidal perturbation

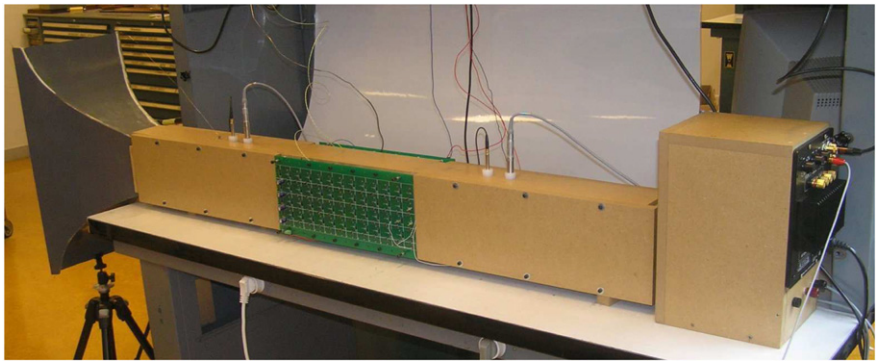

Figure 17. Experimental set-up.

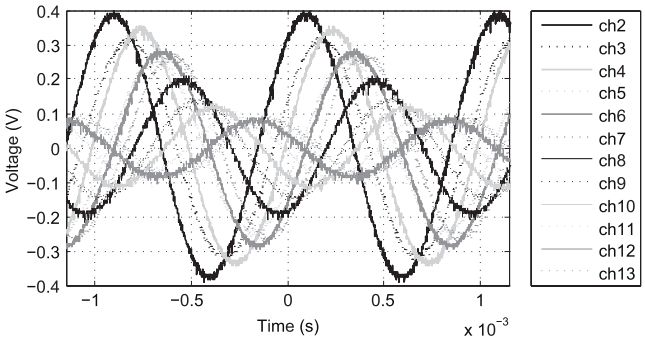

Figure 18. Amplitude and phase on different channels of microphones.

propagates along the microphone channels from the input to the output.

3.4. Experimental results

Only the acoustic transfer functions of the system were studied at this first stage of experimental investigation. Precision acoustic microphones in the input and output segment have enabled the measurement of the frequency response function of the system with and without control. Input excitation on the primary loudspeaker is a white noise in the frequency band between 0 and 5 kHz.

Firstly, we have tested the passive attenuation of the system when the control algorithm is turned off. In figure 19 is shown a comparison of the attenuation when rigid walls are inserted in the tube instead of the active surfaces. It can be seen that the simple replacement of rigid walls by the active system, even without control, brings a significant reduction of the acoustic level. The attenuation effect up to 8 dB is important, especially at low frequencies, where the control speakers cannot offer significant results because of their electromechanical properties (first suspension mode). The almost linear phase evolution confirms correct propagation of the sound wave along the tube.

Figure 20 presents the results when the control system is activated. In addition to passive attenuation at low frequencies, the effect of the control law appears at intermediate frequencies with the maximum of 30 dB in amplitude reduction. The efficient frequency band of the active system is situated between 800 Hz and 1.5 kHz. The lower limit is caused by the first eigenmode of the control speaker and the higher limit by the time delay of calculation process, which becomes more important and leads to the control algorithm losing its efficiency. Nevertheless, there is a significant attenuation even for non-plane waves above 1200 Hz. It is important to note that the total power consumption of the whole system under control does not exceed 30 W, which is negligible compared to other types of fully distributed acoustic control devices.

In figure 21 is shown the sound transmission loss of the control device. The plane waves in this system occur for frequencies below 1270 Hz. In comparison with the previous control device (figure 9), the levels of acoustic power attenuation are more uniform through all the considered frequency band.

4. Conclusion

This paper shows the development and certain numerical and experimental results obtained by a new distributed control system, completely different compared to other methods used up to now. A new methodology for designing control strategies based on a distributed transducer network is presented. With the objective of controlling the acoustic energy transfer through a tube, it has been demonstrated on a simple example the type of results that can be obtained. The numerical modelling has been validated by experimental results. Although these results show clearly the potential benefits, they also present the difficulties of setting up the experimental realization, especially the time and space discretization and electromechanical properties of the actuators used. The obtained results are nevertheless very encouraging, and the robustness, stability and simple implementation of the control law show the potential of such a method.

The presented system has the great merit of being very effective and allows an important attenuation of the acoustic transfer without the necessity of very strong displacements of the membrane interfaces [14]. It is thus possible to use this technique with transducers produced on a silicon base with thin deposits of PZT layers as actuator elements, so the proposed

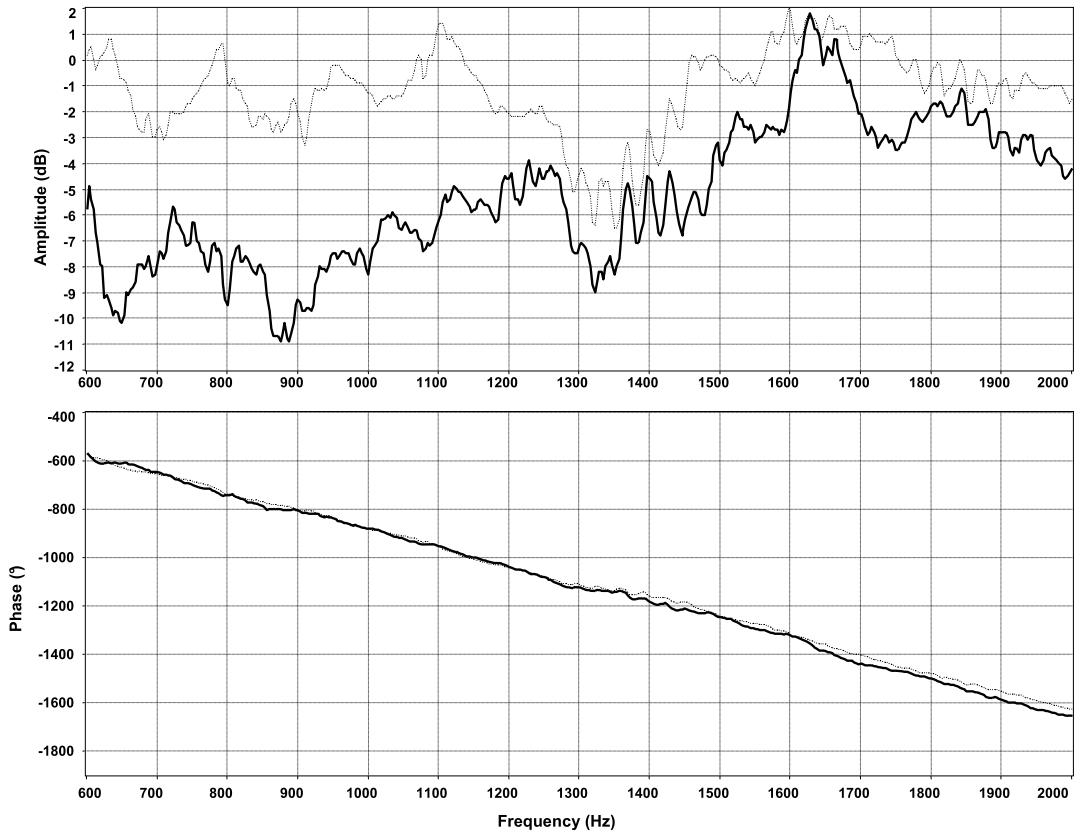

Figure 19. Transfer function between the input and output microphone, — active surfaces without control; · · · chipboard rigid walls.

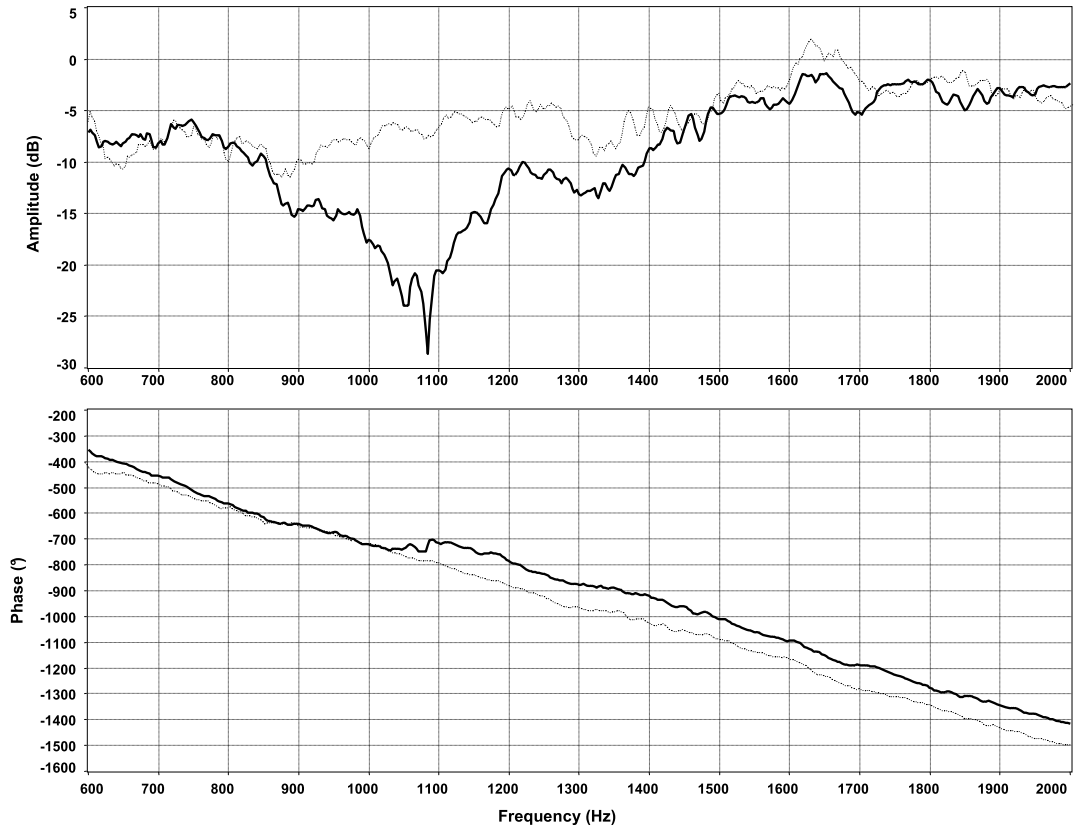

Figure 20. Transfer function between the input and output microphone, — active surfaces with control; · · · without control.

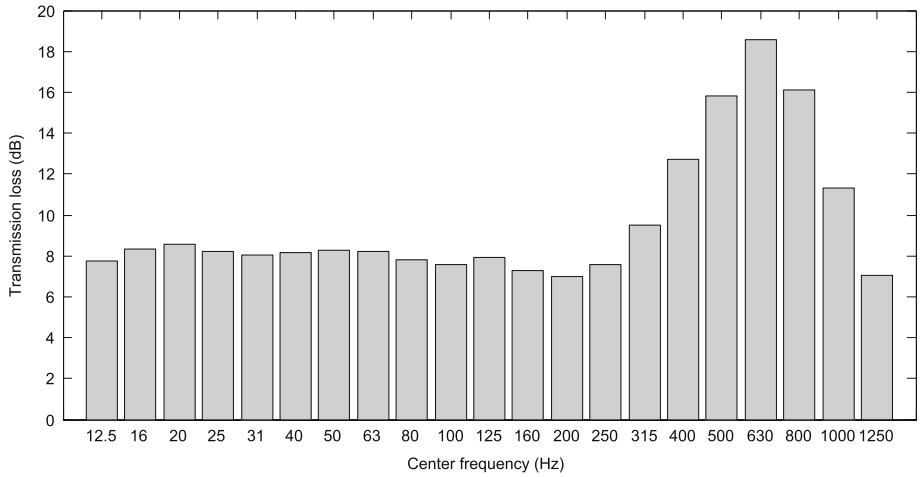

Figure 21. Sound transmission loss in 1/3 octave bands, experimental results.

method appears to be suitable for use with distributed MEMS transducers to reduce noise over a large frequency band.

We have presented the development of individual cells with an integrated microcontroller, sensor and actuator, power supply, signal amplification and conditioning, and especially the possibility of interconnection of many such cells in the area network, a so-called active antinoise skin. The distributed control algorithm of every cell uses as input signal its own sensor and several sensors from neighbouring cells, which is necessary for the implementation of spatial operators. The cells, as well as the entire network, have been validated before testing the global behaviour of the entire system. It has been revealed that the critical parameters for experimental implementation are particularly the first suspension mode of the control speakers and the time delay introduced by the calculation loop. The experimental results clearly show the great potential of this approach, further experimental investigation is however necessary to determine all the system properties and limitations.

References

[1] Atalla N, Panneton R, Sgard F C and Olny X 2001 Acoustic absorption of macro-perforated porous materials *J. Sound Vib.* **243** 659–78

[2] Ramakrishnan R and Watson W R 1992 Design curves for rectangular splitter silencers *Appl. Acoust.* **35** 1–24

[3] Zheng H, Cai C, Pau G S H and Liu G R 2005 Minimizing vibration response of cylindrical shells through layout optimization of passive constrained layer damping treatments *J. Sound Vib.* **279** 739–56

[4] Kostek T M and Franchek M 2000 Hybrid noise control in ducts *J. Sound Vib.* **237** 81–100

[5] Furstoss M, Thenail D and Galland M A 1997 Surface impedance control for sound absorption: direct and hybrid passive/active strategies *J. Sound Vib.* **203** 219–36

[6] Mazeaud B 2005 Developing of an intelligent sound coating for a duct in the presence of flow *PhD Thesis* Laboratory of Fluid Mechanics and Acoustics, Centrale Lyon

[7] Nelson P A and Elliott S J 1992 *Active Control of Sound* (London: Academic)

[8] Guicking D and Karcher K 1984 Active impedance control for one-dimensional sound *ASME J. Vib., Acoust., Stress, Reliab. Des.* **106** 393–96

[9] Galland M A, Mazeaud B and Sellen N 2005 Hybrid passive/active absorbers for flow ducts *Appl. Acoust.* **66** 691–708

[10] Sellen N, Cuesta M and Galland M A 2003 Passive layer optimization for active absorbers in flow duct applications *Ninth AIAA/CEAS Aeroacoustics Conf.,* AIAA paper No. 2003-3186

[11] Matignon D, Audounet J and Montseny G 1998 Smart energy decay for wave equations with damping of fractional order *Fourth Int. Conf. on Mathematical and Numerical Aspects of Wave Propagation Phenomena* pp 638–40

[12] Montseny G 1998 Diffusive representation of pseudo-differential time-operator *ESAIM: Proceedings, Fractional Differential Systems: Models, Methods and Applications* vol 5 pp 159–75

[13] Triggiani R and Lasiecka I 1989 Exact controllability of the wave equation with neumann boundary control *Appl. Math. Optim.* **19** 243–90

[14] Collet M, David P and Berthillier M 2009 Active acoustical impedance using distributed electrodynamical transducers *J. Acoust. Soc. Am.* **125** 882–94

[15] Galucio A C, Deü J F and Ohayon R 2005 A fractional derivative viscoelastic model for hybrid u active–passive damping treatments in time domain–application to sandwich beams *J. Intell. Mater. Syst. Struct.* **16** 33–45

[16] Hilbrunner O 2003 Developing and optimization of an active control system for hybrid acoustic absorbers *PhD Thesis* Centrale Lyon